https://doi.org/10.15407/ujpe68.12.785

V.S. MUKHAROVSKA,[1] M.P. DERHACHOV,[1] V.M. MOISEIENKO,[1] B. ABU SAL[2]

[1] Oles Honchar Dnipro National University
(72, Gagarina Ave., Dnipro 49010, Ukraine; e-mail: derhachov.mp@gmail.com)
[2] Applied Physics Department, Tafila Technical University
(P.O. Box 40, Al-Eis 66141, Tafila, Jordan)

PECULIARITIES OF Eu^{3+} PHOTOLUMINESCENCE IN OPAL PHOTONIC CRYSTAL FILMS AND HETEROSTRUCTURES BASED ON THEM

Single opal films and heterostructures based on them grown by the method of vertically moving meniscus are characterized by the reflection spectroscopy technique and then impregnated with the $Eu(CH_3COO)_3 \times H_2O$ salt. The suppression of the Eu^{3+} ion emission in single opal films is clearly detected within the photonic stop-band range. The weaker manifestation of this effect in heterostructures is more likely due to interface defects causing both the appearance of permitted states in the photonic stop band and the scattering of radiation in the direction of observation. With the further impregnation of opal films with glycerol to reduce the dielectric contrast from 1.85 to 1.13, the emission spectrum is mainly determined by the Eu^{3+} coordination environment effects accompanied with the broadening of bands and the spectral intensity redistribution.

Keywords: synthesis of monodisperse silica particles, opal film, photonic stop band, opal heterostructure, suppression of emission.

1. Introduction

The principles of controlling the emission and propagation of light in artificial dielectric structures with periodic and random variations of the permittivity on the scale of hundreds of nanometers have been outlined in the works by Bykov [1], Yablonovitch [2], and John [3]. Since then, such structures, called photonic crystals (PhCs), have been intensively employed as the basis for creating all-optical circuits, nanophotonic devices [4–6], sensors [7–9], lasers[10–12], antireflection coatings [13], as well as for the molecular recognition [14] and photocatalytic applications [15, 16]. Their main feature is the possibility of forming a specific frequency interval within which there are no permitted states, and electromagnetic waves cannot propagate throughout the PhC due to the destructive interference. It may be realized either in all spatial directions, photonic band gap (PhBG), or in certain crystallographic ones, photonic stop band (PhSB), depending on the dielectric contrast and the structure lattice symmetry [17].

The most promising and suitable materials for creating 3D PhCs with PhBG or PhSB in the visible or near-infrared regions are artificial and inverse opals. Artificial opals are porous matrices composed

Citation: Mukharovska V.S., Derhachov M.P., Moiseienko V.M., Abu Sal B. Peculiarities of Eu^{3+} photoluminescence in opal photonic crystal films and heterostructures based of them. *Ukr. J. Phys.* **68**, No. 12, 785 (2023). https://doi.org/10.15407/ujpe68.12.785.

Цитування: Мухаровська В., Дергачов М., Абу Сал Б. Особливості фотолюмінесценції Eu^{3+} у фотонно-кристалічних опалових плівках та гетероструктурах на їх основі. *Укр. фіз. журн.* **68**, №12, 787 (2023).

of sequential layers of close-packed particles with diameters of hundreds of nanometers. Generally, silica (SiO_2) particles are used [18], but other ones made of polystyrene (PS) or polymethyl methacrylate (PMMA) can also be exploited [19]. To vary the dielectric contrast and to enlarge the functionality of opal PhCs, the matrices are impregnated with magnetic clusters [20, 21], active dielectrics [22–24], semiconductors [25–27],organic and laser-active materials [28–30]. Inverse opals are fabricated by removing PS or PMMA spheres from impregnated matrices [31, 32]. For artificial opals, one should expect the formation of PhSBs, while, for inverted opals, the PhBG appearance is possible in the case of using a higher refractive index filler.

Among different types of opal PhCs, film opals stand out for wider technological abilities of varying their properties, lower defect concentration, and shorter fabrication time [33, 34]. Their planar structure allows one to extend the fields of the PhCs application to the deformation imaging [35], silicon photovoltaics [36], and anti-counterfeiting technology [37] in addition to those already mentioned.

Nevertheless, one of the main existing challenges remains the manipulation of the emission spectrum through varying PhSB parameters and incorporating preassigned defects. Heterostructures based on opal films look very promising for this task. Being composed of opal films with a small difference of particles' sizes, they provide a flexible PhSB modification [38–41], and the interface of two films itself is a defect that can be controlled, as far as the film growth is controlled [42, 43].

Lanthanide rare-earth ions, due to their narrow emission bands, are one of the most suitable candidates for the incorporation into the opal matrix, since their 4f-4f emission can be completely covered by the PhSB. However, most of works devoted to this topic consider the luminescence of lanthanides (Eu, Tb, Er, Tm, Yb) in either bulk artificial opals with the single PhSB [44–48] or inverse opals [49–51].

The aim of this work is to investigate the influence of the photonic stop band on the Eu^{3+} emission spectrum in opal films and heterostructures based on them, as well as the coordination environment effect, when opal films being additionally impregnated with glycerol to decrease the dielectric contrast. For this reason, europium-containing salt, $Eu(CH_3COO)_3 \times H_2O$, is embedded both in single opal films and heterostructures derived from opal films of silica particles with close diameters. The choice of a material is due to its high luminescence efficiency and convenient impregnation technique.

2. Samples Fabrication and Experimental Technique

2.1. Samples fabrication

Monodisperse spherical silica particles (SPs) were synthesized using the modified Stöber–Fink–Bohn (SFB) method by tetraethyl orthosilicate (TEOS) hydrolysis in ethanol–water solution in the presence of ammonia hydroxide [52]. The reaction solutions contained 9–17 M of H_2O, 1–2 M of NH_3, 10–13 M of C_2H_5OH, and 0.14–0.24 M of $SiC_8H_{20}O_4$. Thereupon, SPs were deposited on a glass substrate using the method of vertically moving meniscus. The movement of the meniscus was provided by the slow evaporation of a colloidal suspension. The films obtained in such a way were assumed to have the fcc lattice, formed by SPs, with the lattice direction [111] perpendicular to the film growth surface [53, 54]. The film growth process was carried out under the isothermal conditions at 25 °C with the subsequent annealing at 100 °C for 6 hours to increase the mechanical stability.

For the further formation of the PhC heterostructure, SPs of another diameter were prepared by the multistage SFB method [55]. In this respect, the portion of the above-mentioned suspension was diluted in water–ethano–ammonium mixed solvent of the same compound and an additional quantity of TEOS. The second film of opal heterostructure was crystalized on the first one acting like a substrate using the method mentioned above. Upon the crystallization, both heterostructures and single films were annealed at 450 °C for 3 hours in order to remove physically adsorbed water and organic residues from the opal structure [56].

The infiltration of obtained samples was carried out in a saturated aqueous solution of europium (III) acetate monohydrate salt, $Eu(CH_3COO)_3 \times H_2O$ (Sigma-Aldrich, 99.9%), under the action of capillary forces with the subsequent drying at room temperature. As shown by our previous electron microscopic studies [57], this procedure results in the deposition of the salt in a polycrystalline state on the surface of silica particles. To examine the luminescence under low dielectric contrast conditions, single opal films

with the salt were additionally impregnated with an aqueous glycerol solution.

2.2. Experimental technique

Reflection spectra of both a single film and the two-film heterostructure were measured at different angles θ with respect to a normal to the growth surface, the [111] direction (Fig. 1, *a*). All the spectra were obtained within the 420–650 nm interval. Reflectance coefficients were derived from the corresponding spectra by dividing them by the emission spectrum of an incandescent lamp used for the sample illumination.

Unpolarized photoluminescence (PL) spectra of the $Eu(CH_3COO)_3 \times H_2O$ salt both in an optical cell and in pores of opal-based structures were measured within the 575–625 nm spectral interval. Excitation was performed by a continuous radiation both in the $^5L_6 \leftarrow ^7F_1$ transition band overlapped with the $^5L_6 \leftarrow ^7F_0$ one (a 410 nm semiconductor laser) and in the hypersensitive $^5D_1 \leftarrow ^7F_1$ transition band (a 532 nm diode pumped solid-state laser). Both forward and backward scattering geometries were used for these measurements. In the forward scattering geometry, the salt in the bottom film (film *1*) was firstly excited, and PL spectra were taken from the opposite side of the single film or top film of the heterostructure (film *2*) at the angles $\theta = 0°$, 40 °, and 50° with respect to the [111] direction (Fig. 1, *b*).

All the spectra were analyzed by using a modified laser spectrometer based on a double monochromator DFS-12 with a photon counting system. The laser beam spot diameter on the sample surface was no more than 1.5 μm, and an error in the angle setting did not exceed 1.50. The spectral resolution was 0.5 cm^{-1}, and an accuracy in defining a spectral position was ± 1.0 cm^{-1}.

3. Results and Discussion

3.1. Optical characterization of opal films and heterostructures

The angular dependences of the reflectance spectra of both the film 1, which served as the bottom film in a further heterostructure, and two-film heterostructure are presented in Fig. 2.

Since opal is a structure with a permittivity modulation on the scale of hundreds of nanometers, its reflectance in the visible region is originated from the light Bragg diffraction, the first-order diffraction on

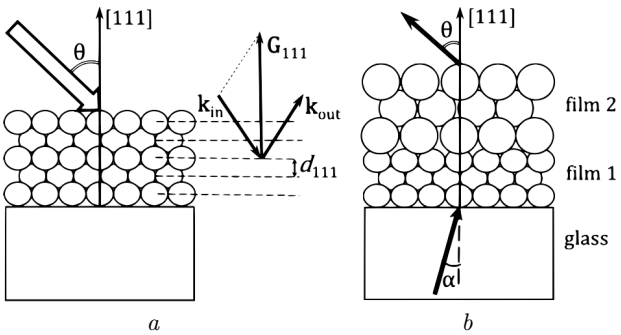

Fig. 1. Reflection (*a*) and photoluminescence (*b*) measurement schemes. The Bragg diffraction diagram, corresponding to the Laue equation $\mathbf{k}_{\rm in} + \mathbf{G}_{hkl} = \mathbf{k}_{\rm out}$, determines the reflection peak parameters for the wavevectors of incoming $\mathbf{k}_{\rm in}$ and outgoing $\mathbf{k}_{\rm out}$ beams in opal, and corresponding reciprocal lattice vector $\mathbf{G}_{hkl}$ (*a*). Photoluminescence is detected on the opposite side of the sample (on the external side of the top film 2) at $\theta = 0°$, 40°, and 50°, when bottom film 1 being excited on the glass substrate side at $\alpha = 15°$ to the [111] direction (*b*)

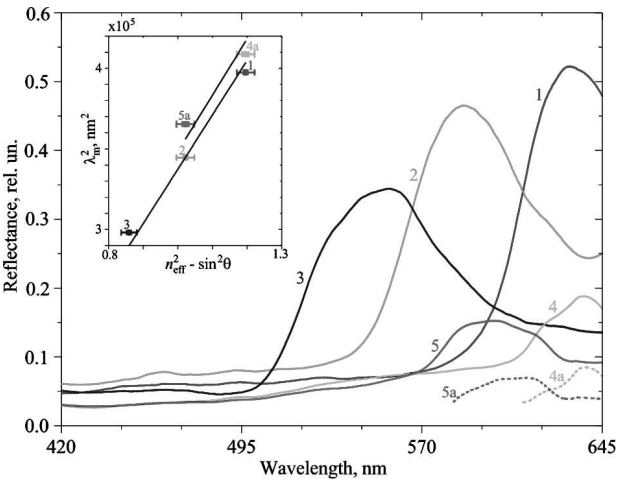

Fig. 2. The film *1* (*1—3*) and two-film heterostructure (*4, 5*) reflectance spectra measured at $\theta = 40°$ (*1, 4*), 50° (*2, 5*), and 60° (*3*). The dashed curves, 4*a* and *5a*, represent the extracted reflectance spectra of the top film (film *2*) at $\theta = 40°$ and 50°, respectively, with considering light scattering at the interface ($\sigma = 0.78$). Solid lines in the inset are linear approximations of the angular dependence of the reflectance maximum position

the (111) planes, in our case. As the Laue equation suggests (Fig. 1, *a*), the angular dependence of the reflectance maximum position λ_m is determined by the interplanar (111) spacing d_{111} and the effective refraction index $n_{\rm eff}$ ($n_{\rm eff} = 1.27$) as follows:

$$\lambda_m = 2d_{111}\left(n_{\rm eff}^2 - \sin^2\theta\right)^{1/2}.$$

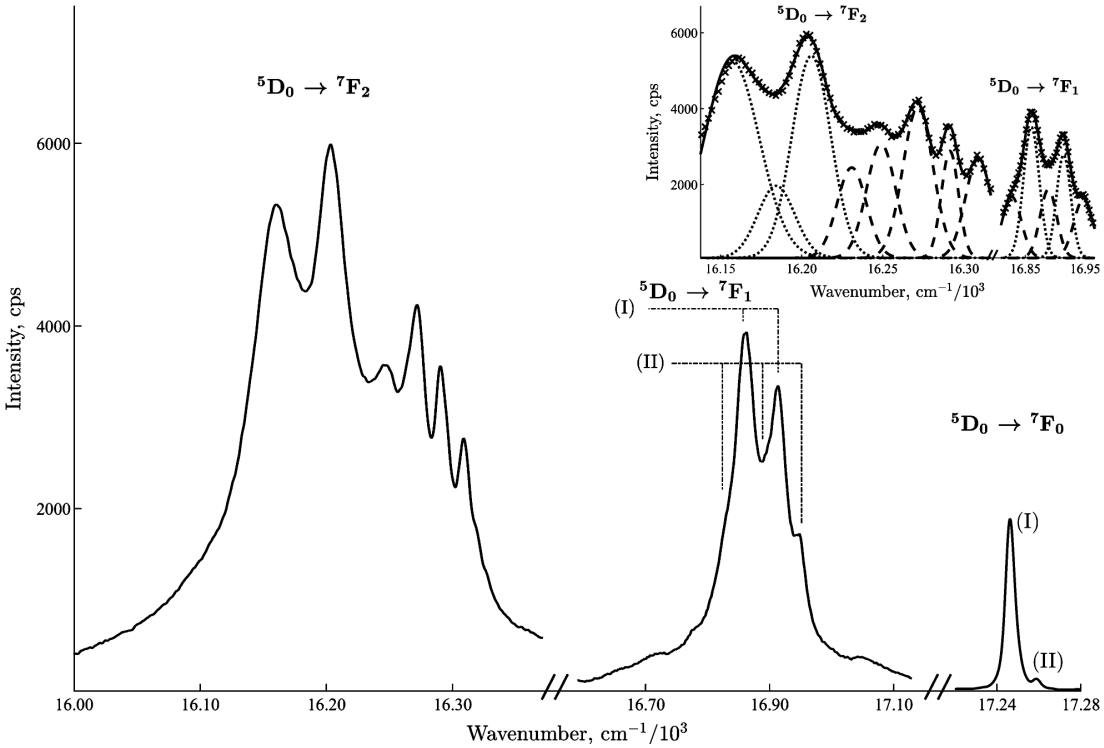

Fig. 3. Photoluminescence spectrum of $Eu(CH_3COO)_3 \times H_2O$ salt in an optical cell. The inset shows the deconvolution by the Gauss functions. Dotted and dashed curves are components related to the (I) and (II) Eu^{3+} site symmetries, respectively. Solid curve is the sum of deconvolution components, cross marks represent the original spectrum

By applying a linear approximation with zero intercept to the experimental data $\{n_{\text{eff}}^2 - \sin^2\theta, \lambda_m^2\}$ (the inset in Fig. 2), the mean SP diameter D can be calculated through $D = (3/2)^{1/2} d_{111}$, $D_1 = 356$ nm in film *1*. The value of the relative reflectance bandwidth, not exceeding 10%, indicates a low dispersion of particle diameters within several nanometers in this film.

As shown by curves *4, 5* in Fig. 2, the reflectance of two-film heterostructure is significantly lower than that of the single film. This may be firstly due to the increase in light scattering at the interface of the two films, which reduces the contribution of the bottom film (film *1*) to the total reflection spectrum. In first approach, the heterostructure reflectance spectrum $R(\lambda, \theta)$ can be represented by a sum of spectra of film *2*, $R_2(\lambda, \theta)$, and film *1*, with considering the previous reflection in film *2* and scattering on the interface between films, $R_1(\lambda, \theta)[1-\sigma]\,[1-R_2(\lambda, \theta)]$. By assuming the scattering coefficient σ to be wavelength independent within the spectral interval under study, we can extract $R_2(\lambda, \theta)$ and estimate the mean SP diameter in film *2* as $D_2 = 362$ nm, according to the procedure described above (the inset in Fig. 2). The low-pronounced profile of the reflectance band of film *2* (curves *4a, 5a* in Fig. 2) is most likely originated from its small thickness and the large number of structural defects, leading to permitted optical states within the PhSB range [58]. The latter is derived from the spectra of films as a bandwidth at the half of the reflectance maximum.

3.2. Interpretation of the $Eu(CH_3COO)_3 \times H_2O$ photoluminescence spectrum

Before examining the PhSB impact on the emission of europium ions in opal structures, we consider the original $Eu(CH_3COO)_3 \times H_2O$ spectrum presented herein on the wavenumber scale for a more convenient analysis of the Stark effect and the contribution of ligand vibrations. As can be seen from Fig. 3, it consists

Deconvolution component parameters

Transition	Peak position (the site type), cm^{-1}	FWHM, cm^{-1}	Component fraction with respect to the integral intensity of the transition band		
	Optical cell		Optical cell	Single film	Two-film heterostructure
$^5D_0 \rightarrow ^7F_1$	16947 (II)	38	0.16	0.09	0.16
	16914 (I)	29	0.24	0.23	0.23
	16888 (II)	35	0.17	0.15	0.18
	16860 (I)	31	0.27	0.41	0.26
	16827 (II)	36	0.16	0.12	0.17
$^5D_0 \rightarrow ^7F_2$	16309 (II)	21	0.08	0.05	0.05
	16291 (II)	17	0.07	0.05	0.10
	16272 (II)	22	0.12	0.11	0.15
	16250 (II)	21	0.09	0.08	0.14
	16234 (II)	21	0.07	0.07	0.07
	16206 (I)	29	0.22	0.27	0.23
	16184 (I)	29	0.08	0.08	0.07
	16162 (I)	39	0.27	0.29	0.19

of three bands centered at 17250 cm^{-1}, 16900 cm^{-1}, and 16200 cm^{-1}, corresponding to the $^5D_0 \rightarrow ^7F_0$, $^5D_0 \rightarrow ^7F_1$, and $^5D_0 \rightarrow ^7F_2$ transitions in the Eu^{3+} spectrum, respectively [59]. As far as the $^7F_0$ and $^5D_0$ levels are non-degenerated, the observation of two $^5D_0 \rightarrow ^7F_0$ emission lines, split by 12 cm^{-1}, suggests that Eu^{3+} ions occupy two non-equivalent sites, labeled (I) and (II), in the host complex.

The presence of two different Eu^{3+} sites is also proved by the Stark splitting pattern of the $^5D_0 \rightarrow ^7F_1$ and $^5D_0 \rightarrow ^7F_2$ transitions, since the number of the emission lines observed for the corresponding spectral regions, at least four and six, respectively (Fig. 3), is obviously greater than the maximum number of crystal-field components predicted for the lowest C_1 symmetry site – three and five [59].

The spectral decomposition performed with the smallest possible number of the Gauss line profiles, considering the equidistant arrangement of the Stark splitting components for each transition, shows the best coincidence for such sets of components as 1, 2, 3 for site (I) and 1, 3, 5 for site (II) (the inset in Fig. 3 and Table). The assignment of the sets to site (I) or (II) is based on the intensities of the spectral components, i.e., more intense lines are associated with site (I) and less intense with site (II).

According to the symmetry analysis and the number of spectral components obtained in each set, site (I) can be attributed to the C_3/C_{3v} point group symmetry. Meanwhile, the observed splitting pattern of Eu^{3+} (II) restricts the feasible point symmetry groups to the following options: C_1, C_s, C_2 or C_{2v}. However, since such type of complexes (Eu acetate hydrates) is typically characterized by the presence of europium sites with specifically C_1 point group symmetry [60, 61], it is suggested that the Eu^{3+} site (II) has also C_1 point group symmetry in our case.

3.3. Photonic stop band and coordination environment effects

The PL spectrum of $Eu(CH_3COO)_3 \times H_2O$ salt in pores of both opal film and heterostructure at $\theta = 0°$, far from the stop band region, does not undergo fundamental changes compared to the original salt spectrum, except for a slight redistribution of the spectral intensity (curves *1*, *4* and *7* in Fig. 4, and Table). With constant, within an accuracy of detection, peak positions and slightly varying half-widths of lines, this redistribution could be explained by the different numbers of Eu^{3+} ions occupying either (I) or (II) site within the excited volume.

In the case of single opal film (film *1*), the emission inhibition effect is clearly detected. The PL intensity in the $^5D_0 \rightarrow ^7F_1$ transition region becomes 1.6 times higher than the intensity in the $^5D_0 \rightarrow ^7F_2$ transition region, which falls in the PhSB region at $\theta = 40°$

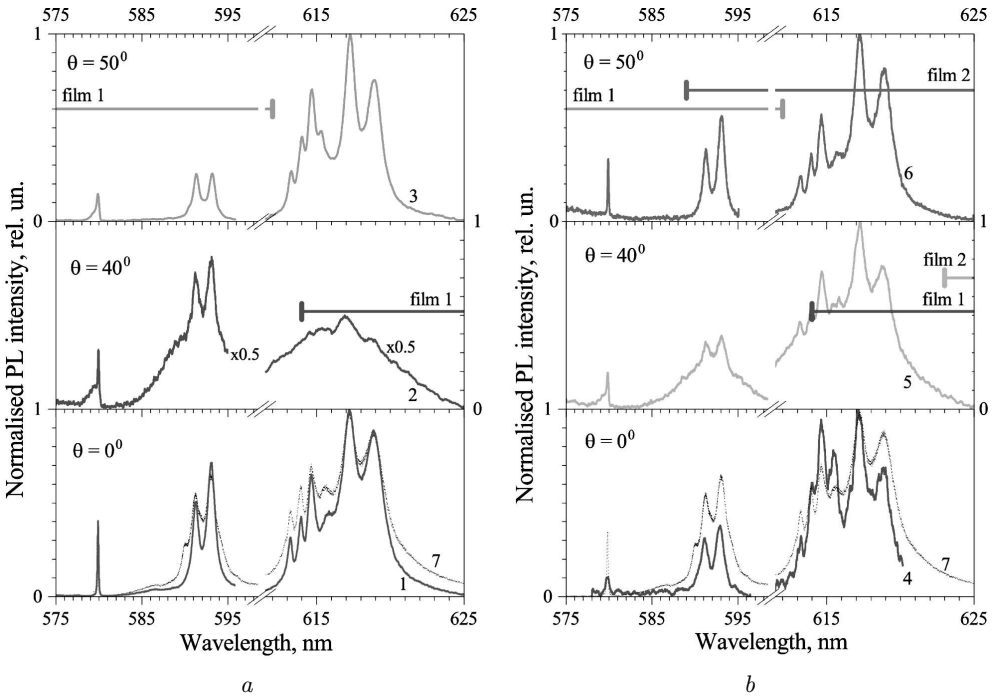

Fig. 4. Photoluminescence spectra of $Eu(CH_3COO)_3 \times H_2O$ salt in pores of the single opal film (*a*) and two-film heterostructure (*b*) measured at different θ relative to the direction [111] and normalized by the intensity value at 617.3 nm. The horizontal bars represent the PhSB region in bottom (film *1*) and top (film *2*) opal films in the heterostructure. Curve *7* is the original spectrum of the salt

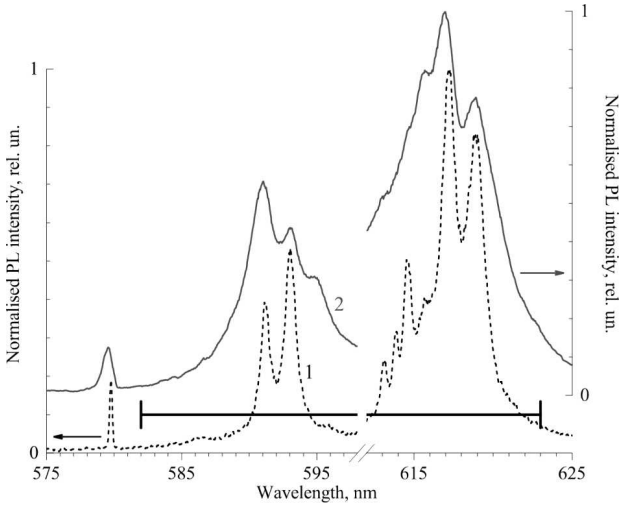

Fig. 5. Photoluminescence spectra of $Eu(CH_3COO)_3 \times H_2O$ salt in pores of the single opal film with the SP diameter $D =$ = 301 nm before (*1*) and after (*2*) the additional impregnation with an aqueous glycerol solution. Both spectra are normalized by the intensity value at 617.3 nm. The horizontal bar represents the PhSB interval in opal before the additional impregnation

(curve *2* and bar in the middle of Fig. 4, *a*). With the following PhSB shift toward the shorter wavelengths at increasing the angle θ, the emission in the region of the $^5D_0 \rightarrow ^7F_0$ and $^5D_0 \rightarrow ^7F_1$ transitions is suppressed, while the relative PL intensity of $^5D_0 \rightarrow ^7F_2$ transition raises (curve *3* and bar at the top of Fig. 4, *a*).

The absence of noticeable changes in the PL spectrum of the salt in heterostructure at non-zero angles of observation may be attributed to the following reasons. According to the measurement scheme (Fig. 1, *b*), the PL spectrum in heterostructure is formed by the successive action of PhSB in films *1* and *2* in the given direction. In the case of $\theta = 40°$, this means that photons with energies, corresponding to the $^5D_0 \rightarrow ^7F_2$ transition, could not already leave film *1* in this direction of observation. At the same time, such photons could easily escape from film *1* in other directions. After the scattering at the interface, they are quite free to propagate in the direction of observation ($\theta = 40°$) in film *2*, since its PhSB is in another spectral interval, and the corresponding op-

tical states are permitted (the middle of Fig. 4, *b*). In the case of $\theta = 50°$, the emission at the $^5D_0 \rightarrow ^7F_0$ transition does not experience a suppression in film *2*, getting there from film *1* due to the scattering at the interface, but the $^5D_0 \rightarrow ^7F_1$ and $^5D_0 \rightarrow ^7F_2$ transitions are in the spectral interval of the PhSB of film *2*, and the corresponding photons could hardly escape from film *2* in the given direction. However, the PhSB effect is weaker than in the single film *1* and manifested by a slight increase in the PL intensities in the regions of the $^5D_0 \rightarrow ^7F_0$ and $^5D_0 \rightarrow ^7F_1$ transitions, the latter being at the PhSB edge (the top of Fig. 4, *b*). This is rather caused by the more disordered structure of film *2*, as mentioned above in the discussion of the reflectance spectra. During the formation of the upper film, silica particles with a larger diameter are deposited on the surface of film *1*, filling all possible positions, including vacancies, and being in a tight contact with the smaller diameter particles in the lower film. This gives rise to a disorder in the structure of the upper film, as it continues to grow, which leads, in turn, to the permitted states in the PhSB, as considered earlier in one-dimensional PhCs [62]. Moreover, the structural irregularities at the interface cause the permitted states in the PhSB of film *1* as well. It allows photons with appropriate energies to leave the lower film in the direction of observation. Thus, the impact of the PhSB of film *1* becomes less pronounced due to the nearby particles of the upper film, acting as point defects in the structure.

Finally, we consider the influence of the additional impregnation of opal-$Eu(CH_3COO)_3 \times H_2O$ sample with an aqueous solution of glycerol (85%). This procedure can be exploited to increase the selectivity of the optical system by narrowing the PhSB region. However, the substance, with which the opal is additionally impregnated, may have a significant effect on the emission properties of the source inside the opal.

As can be seen from Fig. 5, the Eu^{3+} emission spectrum in the initial opal-$Eu(CH_3COO)_3 \times H_2O$ sample is almost completely overlapped by the PhSB region. The impregnation results in decreasing the dielectric contrast from 1.85 to 1.13 and, consequently, in shifting the PhSB center position to the longer wavelengths (from 603 nm to 633 nm) with its narrowing (from 41 nm to 24 nm). This means that, for the shorter wavelength, the PhSB edge is 621 nm, and the PhSB effect on the emission spectrum should not be expected.

The essential broadening of emission lines together with the spectral intensity redistribution (especially for the $^5D_0 \rightarrow ^7F_1$ transition region) observed in the spectrum (curve *2* in Fig. 5) can be explained by the impact of the impregnant on the surroundings of europium ions. As the $^5D_0 \rightarrow ^7F_1$ transition is a magnetic dipole transition, reflecting the splitting of the $^7F_1$ level by the crystal field, the redistribution may be indicative of a lowered symmetry in the Eu^{3+} environment and a change in its polarizability. The broadening, in turn, reveals the disordering of the ligands around europium ions.

4. Conclusions

The original emission spectrum of the Eu (III) acetate monohydrate, $Eu(CH_3COO)_3 \times H_2O$, used for testing the photonic crystal effects, can be well described by assuming the existence of two types of Eu^{3+} sites with the C_3/C_{3v} and C_1 point group symmetries. The Stark splitting of the $^7F_1$ and $^7F_2$ levels for each of these sites is 54 cm^{-1} and 22 cm^{-1}, 60 cm^{-1} and 19 cm^{-1}, respectively. The emission spectrum of the salt embedded into opal pores, measured far from the PhSB region, reveals no essential modification, except for some intensity redistribution caused by a variation in concentrations of the different Eu^{3+} sites.

The weak suppression of the luminescence radiation in the heterostructure of two opal films with similar silica particle diameters can be explained by the following reasons. First, this is the weakening of the contribution to the luminescence from the lower film due to the diffuse scattering on the structure of the interface and the structure of the front film. Second, the formation of the upper film occurred on the profile of the lower one, which led to an increase in the concentration of defects in the upper film and, accordingly, the permitted photonic states in the band gap. Finally, considering the first two factors with the used excitation geometry, the contribution to the luminescence is due to the upper film, the band gap of which is filled with permitted states and does not significantly affect the luminescence intensity of europium ions.

The additional impregnation of the opal film – $Eu(CH_3COO)_3 \times H_2O$ sample with an aqueous solution of glycerol (85%) results in the essential broadening of emission lines and the spectral intensity redistribution. Both effects are attributed to the changes

in the Eu^{3+} coordination environment after the impregnation. The suggestion is that the ligands are disordered, and the polarizability of the medium surrounding europium ions in the pores of the film opal is changed.

1. V.P. Bykov. Spontaneous emission from a medium with a band spectrum. *Sov. J. Quantum Electron.* **4**, 861 (1975).
2. E. Yablonovitch. Inhibited spontaneous emission in solid-state physics and electronics. *Phys. Rev. Lett.* **58**, 2059 (1987).
3. S. John. Strong localization of photons in certain disordered dielectric superlattices. *Phys. Rev. Lett.* **58**, 2486 (1987).
4. M.A. Butt, S.N. Khonina, N.L. Kazanskiy. Recent advances in photonic crystal optical devices: A review. *Opt. Laser Technol.* **142** (2021).
5. A. Sharma, K. Goswami, H. Mondal, T. Datta, M. Sen. A review on photonic crystal based all-optical logic decoder: Linear and nonlinear perspectives. *Opt. Quantum Electron.* **54**, 90 (2022).
6. X.T. He, C.H. Guo, G.J. Tang, M.Y. Li, X.D. Chen, J.W. Dong. Topological polarization beam splitter in dual-polarization all-dielectric valley photonic crystals. *Phys. Rev. Appl.* 18, (2022).
7. A.S. Kuchyanov, P.A. Chubakov, A.I. Plekhanov. Highly sensitive and fast response gas sensor based on a light reflection at the glass-photonic crystal interface. *Opt. Commun.* **351**, 109 (2015).
8. F. Gallego-Góimez, M. Morales, A. Blanco, C. López. Bare silica opals for real-time humidity sensing. *Adv. Mater. Technol.* **4**, 1800493 (2019).
9. T. Li, G. Liu, H. Kong, G. Yang, G. Wei, X. Zhou. Recent advances in photonic crystal-based sensors. *Coord. Chem. Rev.* **475**, 31 (2023).
10. M. Gaio, M. Peruzzo, R. Sapienza. Tuning random lasing in photonic glasses. *Opt. Lett.* **40**, 1611 (2015).
11. S. Kedia, S. Sinha. Random lasing from dyed polystyrene spheres in disordered environments. *J. Laser Appl.* **30**, (2018).
12. Y. Fu, T. Zhai. Distributed feedback organic lasing in photonic crystals. *Front. Optoelectron.* **13**, 18 (2020).
13. J. Wang, J. Zhou, K. Adelihan, F. Shen, H. Li. Antireflection films based on large-area 2D hollow SiO_2 spheres monolayer opals. *J. Inorg. Organomet. Polym. Mater.* **29**, 72 (2019).
14. L. Li, J. Li, J. Xu, Z. Liu. Recent advances of polymeric photonic crystals in molecular recognition. *Dye. Pigment.* **205**, (2022).
15. A. Lonergan, C. O'Dwyer. Many facets of photonic crystals: From optics and sensors to energy storage and photocatalysis. *Adv. Mater. Technol.* **8**, 2201410 (2022).
16. Q. Sun, B. Zhang, Y. He, L. Sun, P. Hou, Z. Gan, L. Yu, L. Dong. Design and synthesis of black phosphorus quantum dot sensitized inverse opal TiO_2 photonic crystal with outstanding photocatalytic activities. *Appl. Surf. Sci.* **609**, 155442 (2023).
17. J.D. Joannopoulos, S.G. Johnson, J.N. Winn, R.D. Meade. *Photonic Crystals: Molding the Flow of Light* (Princeton University Press, 2008) [ISBN: 978-0-6911-2456-8].
18. S.A. Estrada Alvarez, I. Guger, J. Febbraro, A. Turak, H.R. Lin, Y. Salinas, O. Brüggemann. Synthesis and spatial order characterization of controlled silica particle sizes organized as photonic crystals arrays. *Materials (Basel)* **15**, 5864 (2022).
19. M. Matamoros-Ambrocio, E. Sánchez-Mora, E. Gómez-Barojas, J.A. Luna-López. Synthesis and study of the optical properties of PMMA microspheres and opals. *Polymers (Basel)* **13**, 2171 (2021).
20. D.A. Kurdyukov, A.B. Pevtsov, A.N. Smirnov, M.A. Yagovkina, V.Y. Grigorev, V.V. Romanov, N.T. Bagraev, V.G. Golubev. Formation of three-dimensional arrays of magnetic clusters NiO, Co_3O_4, and $NiCo_2O_4$ by the matrix method. *Phys. Solid State.* **58**, 1216 (2016).
21. E.Y. Stovpiaga, D.A. Eurov, D.A. Kurdyukov, A.N. Smirnov, M.A. Yagovkina, V.Y. Grigorev, V.V. Romanov, D.R. Yakovlev, V.G. Golubev. The synthesis of clusters of iron oxides in mesopores of monodisperse spherical silica particles. *Phys. Solid State.* **59**, 1623 (2017).
22. A.B. Sal, V. Moiseyenko, M. Dergachov, A. Yevchik, G. Dovbeshko. Manifestation of metastable γ-TeO_2 phase in the Raman spectrum of crystals grown in synthetic opal pores. *Ukr. J. Phys. Opt.* **14**, 119 (2013).
23. V.S. Gorelik, D. Bi, G.T. Fei. Optical properties of mesoporous photonic crystals, filled with dielectrics, ferroelectrics and piezoelectrics. *J. Adv. Dielectr.* **7**, 1750038 (2017).
24. M. Derhachov, V. Moiseienko, N. Kutseva, B. Abu Sal, R. Holze, S. Pliaka, A. Yevchyk. Structure, optical and electric properties of opal-bismuth silicate nanocomposites. *Acta Phys. Pol. A* **133**, 847 (2018).
25. S.S. Kurbanov, T.W. Kang. Photoluminescence properties of bare and ZnO infilled artificial opal. *Opt. Commun.* **282**, 2040 (2009).
26. V.G. Golubev. Three-dimensional photonic crystals based on opal-semiconductor and opal-metal nanocomposites. *NATO Sci. Peace Secur. Ser. B Phys. Biophys.* 101 (2010).
27. M. Kepińska, A. Starczewska, I. Bednarczyk, J. Szala, P. Szperlich, K. Mistewicz. Fabrication and characterisation of SbI_3-opal structures. *Mater. Lett.* **130**, 17 (2014).
28. O.K. Alimov, T.T. Basiev, Y.V. Orlovskii, V.V. Osiko, M.I. Samoilovich. Conversion of the luminescence of laser dyes in opal matrices to stimulated emission. *Quantum Electron.* **38**, 665 (2008).
29. V. Moiseyenko, M. Dergachov, A.B. Sal, A. Yevchik. Modification of optical properties of 2,5-bis(2-benzoxazolyl)hydroquinone in opal photonic crystals. *Ukr. J. Phys. Opt.* **14**, 225 (2013).
30. Y. Nishijima, S. Juodkazis. Optical characterization and lasing in three-dimensional opal-structures. *Front. Mater.* **2**, 49 (2015).

31. J. Yu, J. Lei, L. Wang, J. Zhang, Y. Liu. TiO_2 inverse opal photonic crystals: Synthesis, modification, and applications – A review. *J. Alloys Compd.* **769**, 740 (2018).
32. P.S. Hung, C.H. Liao, B.H. Huang, W.A. Chung, S.Y. Chang, P.W. Wu. Formation of free-standing inverse opals with gradient pores. *Nanomaterials.* **10**, 1923 (2020).
33. E.V. Panfilova, V.A. Dyubanov. Automation of the opal colloidal films obtaining processes. In: *Advances in Automation. RusAutoCon 2019. Lecture Notes in Electrical Engineering. Springer* **641**, 2020, p. 1044.
34. M. Muldarisnur, F. Marlow. Structure and optical properties of opal films made by an out-of-plane electric field-assisted capillary deposition method. *ACS Omega.* **7**, 8084 (2022).
35. Z. Yang, M. Koyama, H. Fudouzi, T. Hojo, E. Akiyama. Availability of opal photonic crystal films for visualizing heterogeneous strain evolution in steels: Example of Lüders deformation. *Tetsu-to-Hagane.* **107**, 681 (2021).
36. P.G. O'Brien, N.P. Kherani, A. Chutinan, G.A. Ozin, S. John, S. Zukotynski. Silicon photovoltaics using conducting photonic crystal back-reflectors. *Adv. Mater.* **20**, 1577 (2008).
37. T. Winter, A. Boehm, V. Presser, M. Gallei. Dye-loaded mechanochromic and pH-responsive elastomeric opal films. *Macromol. Rapid Commun.* **42**, 2000557 (2021).
38. S.G. Romanov. Optical characterisation of opal photonic hetero-crystals. *NATO Sci. Ser. II Math. Phys. Chem.* 309 (2004).
39. W. Khunsin, S.G. Romanov, C.M. Sotomayor Torres, J. Ye, R. Zentel. Optical transmission in triple-film heteroopals. *J. Appl. Phys.* **104**, 013527 (2008).
40. A.Z. Khokhar, F. Rahman, N.P. Johnson. Photonic crystal heterostructures from self-assembled opals. *Appl. Phys. A Mater. Sci. Process.* **102**, 281 (2011).
41. L. Zhang, B. Liu, J. Wang, S. Tao, Q. Yan. A general strategy to fabricate photonic crystal heterostructure with Programmed photonic stopband. *J. Colloid Interface Sci.* **509**, 318 (2018).
42. D. Boyang, M. Bardosova, I. Povey, M.E. Pemble, S.G. Romanov. Transmission spectrum transformation at photonic hetero-crystal interfaces – Polarization anisotropy. In: *10th Anniversary International Conference on Transparent Optical Networks, Athens, Greece, 2008*, p. 68.
43. D.A. Eurov, D.A. Kurdyukov, E.Y. Trofimova, S.A. Yakovlev, L.V. Sharonova, A.V. Shvidchenko, V.G. Golubev. Preparation of colloidal films with different degrees of disorder from monodisperse spherical silica particles. *Phys. Solid State.* **55**, 1718 (2013).
44. V.S. Gorelik, S.N. Ivicheva, L.S. Lepnev, A.O. Litvinova, V.N. Moiseenko. Emission of opal photonic crystals filled with europium and terbium. *Inorg. Mater.* **51**, 525 (2015).
45. V.S. Gorelik, L.S. Lepnev, A.O. Litvinova. Photoluminescence of terbium nitrate hexahydrate incorporated into pores of opal photonic crystals. *Inorg. Mater.* **53**, 847 (2017).
46. Y. Shi, F. Zhang, J. Xu, K. Zhou, C. Chen, J. Cheng, P. Li. Upconversion fluorescence enhancement of $NaYF_4:Yb/Re$ nanoparticles by coupling with SiO_2 opal photonic crystals. *J. Mater. Sci.* **54**, 8461 (2019).
47. X. Zhang, H. Zhang, Y.-J. Li. Enhancement of the upconversion luminescence of $ZnO:Yb^{3+}/Er^{3+}$ by photonic crystals. *Optoelectron. Lett.* **15**, 195 (2019).
48. V.N. Moiseienko, V.S. Gorelik, B.A. Sal, O.V. Ohiienko, D.O. Golochalov. Luminescent properties of nanocomposite-$Bi_{12}SiO_{20}$, filled with $C_6H_9EuO_6 \times H_2O$. *J. Phys. Conf. Ser.* **1348**, 012096 (2019).
49. Y. Wang, W. Xu, S. Cui, S. Xu, Z. Yin, H. Song, P. Zhou, X. Liu, L. Xu, H. Cui. Highly improved upconversion luminescence in $NaGd(WO_4)_2:Yb^{3+}/Tm^{3+}$ inverse opal photonic crystals. *Nanoscale.* **7**, 1363 (2015).
50. Z. Chai, Z. Yang, A. Huang, C. Yu, J. Qiu, Z. Song. Preparation and upconversion luminescence modification of $YbPO_4:Er^{3+}$ inverse opal heterostructure. *J. Rare Earths.* **35**, 1180 (2017).
51. Y. Ren, Z. Yang, M. Li, J. Qiu, Z. Song, D. Zhou, B. Liu. Upconversion luminescence modification induced near infrared luminescence enhancement of $Bi_2Ti_2O_7:Yb^{3+}$, Er^{3+} inverse opals. *J. Lumin.* **208**, 150 (2019).
52. W. Stöber, A. Fink, E. Bohn. Controlled growth of monodisperse silica spheres in the micron size range. *J. Colloid Interface Sci.* **26**, 62 (1968).
53. A.V. Baryshev, A.A. Kaplyanskii, V.A. Kosobukin, K.B. Samusev, D.E. Usvyat, M.F. Limonov. Photonic band-gap structure: From spectroscopy towards visualization. *Phys. Rev. B – Condens. Matter Mater. Phys.* **70**, 113104 (2004).
54. A.S. Sinitskii, A.V. Knot'ko, Y.D. Tretyakov. Silica photonic crystals: synthesis and optical properties. *Solid State Ionics.* **172**, 477 (2004).
55. V.M. Masalov, N.S. Sukhinina, G.A. Emel'chenko. Colloidal particles of silicon dioxide for the formation of opal-like structures, *Phys. Solid State.* **53**, 1135 (2011).
56. É.N. Samarov, A.D. Mokrushin, V.M. Masalov, G.E. Abrosimova, G.A. Emel'chenko. Structural modification of synthetic opals during thermal treatment. *Phys. Solid State.* **48**, 1280 (2006).
57. O. V. Ohiienko, V.N. Moiseyenko, T.V. Shvets. Luminescent properties of europium (III) acetate monohydrate in synthetic opal pores. *Mol. Cryst. Liq. Cryst.* **701**, 72 (2020).
58. A. Yevchik, V. Moiseyenko, M. Dergachov. The influence of structural defects on the optical properties of synthetic opals. *Ukr. J. Phys. Opt.* **16**, 24 (2015).
59. K. Binnemans. Interpretation of europium(III) spectra. *Coord. Chem. Rev.* **295**, 1 (2015).
60. S. Ganapathy, V.P. Chacko, R.G. Bryant, M.C. Etters. Carbon CP-MASS NMR and X-ray crystal structure of paramagnetic lanthanide acetates. *J. Am. Chem. Soc.* **108**, 3159 (1986).
61. S.G. Torres, I. Pantenburg, G. Meyer. Direct oxidation of europium metal with acetic acid: An-

hydrous europium(III) acetate, $Eu(OAc)_3$, its sesquihydrate, $Eu(OAc)_3(H_2O)_{1.5}$, and the "hydrogendiacetate", $[Eu(H(OAc)_2)_3](H_2O)$. *Zeitschrift Fur Anorg. Und Allg. Chemie.* **632**, 1989 (2006).

62. M.A. Kaliteevskii, V.V. Nikolaev, R.A. Abram. Eigenstate statistics and optical properties of one-dimensional disordered photonic crystal. *Phys. Solid State.* **47**, 1948 (2005).

Received 25.07.23

В. Мухаровська, М. Дергачов, Білял Абу Сал

ОСОБЛИВОСТІ ФОТОЛЮМІНЕСЦЕНЦІЇ Eu^{3+} У ФОТОННО-КРИСТАЛІЧНИХ ОПАЛОВИХ ПЛІВКАХ ТА ГЕТЕРОСТРУКТУРАХ НА ЇХ ОСНОВІ

Одношарові опалові плівки та гетероструктури, отримані за допомогою методу рухомого меніска, були охарактеризовані методами оптичної спектроскопії з подальшою їх інфільтрацією сіллю $Eu(CH_3COO)_3 \cdot H_2O$. В одношарових плівках чітко спостерігається пригнічення випромінювання іонів Eu^{3+} в області, що відповідає фотонній стоп-зоні. Менш виражений прояв цього ефекту у гетероструктурах, ймовірно, зумовлений дефектами на межі інтерфейсу двох плівок, що приводять як до появи дозволених станів у фотонній стоп-зоні, так і до розсіювання випромінювання у напрямку спостереження. Після інфільтрації плівок гліцерином для зниження діелектричного контрасту від 1,85 до 1,13, спектр випромінювання, головним чином, визначається впливом координаційного оточення іонів Eu^{3+}, що виявляється у розширенні смуг люмінісценції та перерозподілі спектральної інтенсивності випромінювання.

Ключові слова: синтез монодисперсних частинок кремнезему, опалова плівка, фотонна стоп-зона, опалова гетероструктура, пригнічення випромінювання.